Does CO_2 Oxidize Ni Catalysts? A Quick X-ray Absorption Spectroscopy Answer

Valentijn De Coster, Nadadur Veeraraghavan Srinath, Parviz Yazdani, Hilde Poelman and Vladimir V. Galvita*

AUTHOR ADDRESS

Valentijn De Coster – Laboratory for Chemical Technology, Ghent University, Technologiepark 125, B-9052 Ghent, Belgium

Nadadur Veeraraghavan Srinath – Laboratory for Chemical Technology, Ghent University, Technologiepark 125, B-9052 Ghent, Belgium

Parviz Yazdani – Laboratory for Chemical Technology, Ghent University, Technologiepark 125, B-9052 Ghent, Belgium

Hilde Poelman – Laboratory for Chemical Technology, Ghent University, Technologiepark 125, B-9052 Ghent, Belgium

Vladimir V. Galvita – Laboratory for Chemical Technology, Ghent University, Technologiepark 125, B-9052 Ghent, Belgium

AUTHOR INFORMATION

***Corresponding Author**

Hilde Poelman – Laboratory for Chemical Technology, Ghent University, Technologiepark 125, B-9052 Ghent, Belgium; E-mail: Hilde.Poelman@UGent.be

ABSTRACT

$MgAl_2O_4$-supported Ni materials are highly active and cost-effective CO_2 conversion catalysts, yet their oxidation by CO_2 remains dubious. Herein, Ni/$MgAl_2O_4$, prepared via colloidal synthesis (10wt% Ni) to limit size distribution, or wet impregnation (5, 10, 20 and 40wt% Ni), and bare, i.e. unsupported, NiO are examined in H_2 reduction and CO_2 oxidation, using thermal conductivity detector based measurements and in-situ quick X-ray absorption spectroscopy, analyzed via chemometrics. Ni re-oxidation does not occur for bare Ni, but is observed solely on supported materials. Only samples with smallest particle sizes get fully re-oxidized. The Ni-$MgAl_2O_4$ interface, exhibiting metal-support interactions, activates CO_2 and channels oxygen into the reduced lattice. Oxygen diffuses inwards, away from the interface, oxidizing Ni entirely or partially, depending on the particle size in the applied oxidation timeframe. This work evidences Ni oxidation by CO_2, explores the conditions of its occurrence and the importance of metal-support effects.

KEYWORDS: Quick-XAS, Ni-based catalyst, role of support, redox properties, metal-support interaction

TOC GRAPHICS

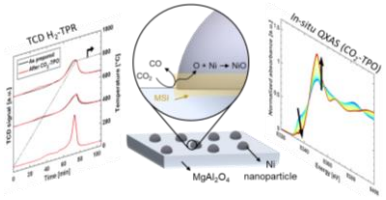

CO_2 utilization, i.e. converting CO_2 into useful chemical products, is indispensable to mitigate rising greenhouse gas concentrations and ensure sustainable development. Within this context, employing CO_2 as reagent in catalytic gas-phase reactions, e.g. methane dry reforming[1-3] and CO_2 hydrogenation[4-6], has received increased attention over the past years. Supported Ni materials[7-14] are particularly effective catalysts for CO_2 utilization, owing to their high activity and cost-effectiveness compared to noble metal-based alternatives[3]. Despite their interesting properties, several fundamental open questions remain for these catalytic Ni systems, which impede their improvement and industrial implementation. One such question is the interaction of CO_2 with Ni, particularly the capacity of CO_2 to oxidize Ni. Addressing this Ni-CO_2 interplay is nevertheless crucial as it determines whether to include Equation 1 in reaction schemes -and associated kinetic models- for Ni-based CO_2 catalysts.

$$CO_2 + Ni \rightarrow NiO + CO \quad \Delta G°_{800°C} = 46 \text{ kJ mol}^{-1} \qquad (1)$$

Generally, Ni oxidation by CO_2 is neglected, given its unfavorable thermodynamics. However, since Ni-based catalysts typically consist of supported Ni nanoparticles (NPs), finite size effects[15] and metal-support interactions[16-19] (MSI) can affect the electronic properties of the prevalent Ni phases, thus enhancing the reactivity of Ni towards CO_2. At present, dedicated experimental studies on the possible oxidation by CO_2 of supported Ni are either contradictory or lacking altogether. Studies of Ni supported on yttrium-stabilized zirconium oxide[20] did not show Ni oxidation by CO_2. In addition, Wierzbicki and co-workers[21] observed no Ni re-oxidation of hydrotalcite-derived Ni materials upon CO_2 exposure. Similarly, Lee et al.[22] observed no notable oxidation of Ni/Al_2O_3 under CO_2 temperature-programmed oxidation (CO_2-TPO). However, Shen and co-workers[23] did report oxidation of Ni/Al_2O_3 under CO_2-TPO. Mutz et al.[24] applied H_2 feed interruptions to CO_2 methanation experiments on Ni/Al_2O_3, and observed that re-oxidation occurred, which was ascribed to CO_2, traces of H_2O or oxygen. Ni oxidation was also observed by Chen et al.[25] for Ni/Al_2O_3 and Ni/$CeAlO_3$-Al_2O_3. Keeping

in mind the materials and pressure gap, near-ambient pressure (<mbar) X-ray photoelectron spectroscopy studies on the interaction of CO_2 with Ni(111)[26] revealed that surface Ni oxidation occurred at room temperature and that this oxidation was more thorough at higher temperatures. To address these ambiguities, a systematic redox study of bare and $MgAl_2O_4$-supported Ni (Ni/$MgAl_2O_4$) is presented. The $MgAl_2O_4$ support was chosen for its industrial relevance[27-28], chemical stability[29] and the high activity reported for Ni/$MgAl_2O_4$ in CO_2 utilization[13, 30-33]. CO_2 oxidation of Ni has been examined using a combination of thermal conductivity detector (TCD)-based H_2 temperature-programmed reduction (H_2-TPR) and CO_2-TPO, as well as in-situ by quick X-ray absorption spectroscopy (QXAS) during H_2-TPR and CO_2-TPO with statistical analysis.

$MgAl_2O_4$ was synthesized via a coprecipitation method[13]. Ni/$MgAl_2O_4$ with 10wt% nominal Ni loading was prepared by colloidal synthesis, based on the work of Vrijburg et al.[34]. This method was chosen as it yields monodisperse NP size distributions, limiting the size-dependent spread on the results[35] (Figure S1). In addition, Ni/$MgAl_2O_4$ materials with targeted 5, 10, 20 and 40wt% Ni were prepared via a 'conventional' wet impregnation (WI) route for comparison. Experimental details are provided in the Supporting Information (SI; section 1). Elemental analysis via scanning electron microscopy with energy-dispersive X-ray spectroscopy analysis (Table S1) indicated the metal contents of all materials were close to their nominal value. Hereafter, the nomenclature C-10Ni/$MgAl_2O_4$ and WI-xNi/$MgAl_2O_4$ (x = 5, 10, 20 or 40) will be used for the colloidal, respectively, WI samples. X-ray diffraction (XRD; Figure S2) and transmission electron microscopy (TEM; Figure S3) results are summarized in Table S1.

QXAS measurements tracked the behavior during H_2-TPR and CO_2-TPO for bulk NiO and monodisperse C-10Ni/$MgAl_2O_4$. The Ni K-edge X-ray absorption near-edge spectra (XANES) of bulk NiO during H_2-TPR show a NiO initial state (Figure 1A). In accordance with the large crystallite size (Table S1), extended X-ray absorption fine structure (EXAFS) analysis (Figure

S4, Table S2) yields a Ni-Ni coordination number (CN) of 12.6±1.4 at a distance of 2.96±0.01Å, which is –within error– identical to that of bulk FCC NiO. During H_2-TPR, reduction to Ni^0 takes place, evidenced by the decrease in white line intensity, the shift of the edge to lower energies and the evolution of the pre-edge from isolated peak to shoulder. Principal component analysis (PCA) derives 4 principal components (PCs), suggesting the presence of more phases than NiO and Ni (Figure S5). However, multivariate curve resolution-alternating least squares (MCR-ALS) (Figure 1B-C) and EXAFS analysis of the derived components (Figure S6) prove that these actually pertain to 2 NiO and 2 Ni components. This deduplication originates from temperature effects, i.e. the Debye-Waller factor, dominating the QXAS spectra when no reduction takes place. The actual reduction occurs in the 'middle' range of the temperature program, i.e. 350–550°C. Spectra recorded below and above this window add thermal variance to the XAS data, which is detected by PCA and MCR-ALS. Consequently, lower (NiO-1, Ni-1) and higher temperature components (NiO-2, Ni-2) are derived for both NiO and Ni (Figure S6). Taking into account this identification and the MCR-ALS concentration profiles (Figure 1C), full reduction of NiO occurs in the range 350–550°C without intermediates formation.

Exposure of the reduced material to CO_2 at 800°C induced no notable spectral changes (Figure 1D), confirmed by PCA (Figure S7). EXAFS modelling of room temperature (RT) spectra after CO_2 treatment (Figure 1E, Table S2) only resolves Ni^0. Hence, no notable Ni oxidation by CO_2 occurred at 800°C for bulk Ni, corroborating thermodynamic calculations.

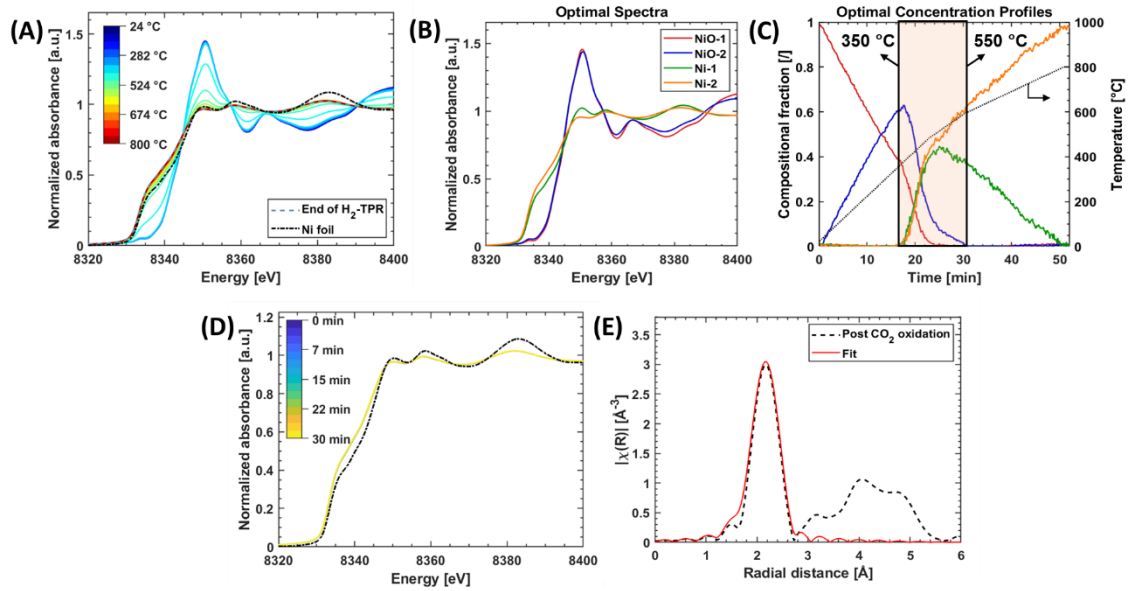

Figure 1. In-situ Ni K-edge QXAS for bulk NiO. (A) XANES during H_2-TPR. (B) MCR-ALS component spectra and (C) concentration profiles, extracted from the QXAS H_2-TPR dataset. Light orange: reduction window, vertical black lines: temperature borders. (D) XANES during isothermal CO_2 oxidation of reduced bulk NiO. (E) Fourier transform of the k^2-weighted EXAFS signal (black) and the fit (red) of reduced bulk NiO after CO_2 oxidation.

XANES of C-10Ni/$MgAl_2O_4$ initially correspond to NiO, in line with XRD (Figure S2) and confirmed by EXAFS fitting (Figure S8, Table S3). The CN of 8.1±1.4 found for Ni-Ni scattering is substantially lower than the bulk value of 12, proving the material's nanoparticulate size, in agreement with TEM (Figure S3A). When exposed to H_2-TPR up to 800°C, reduction of NiO in C-10Ni/$MgAl_2O_4$ occurs, similar to bulk NiO (Figure 2A). PCA reveals 3 PCs (Figure S9), which MCR-ALS (Figure 2B-C) and EXAFS modelling (Figure S10, Table S3) relate to 2 NiO-components (NiO-1, NiO-2) and 1 Ni component (Ni). This number differs from bulk NiO because NiO reduction now predominantly takes place at the end of the temperature program. Hence, Debye-Waller effects dominate the initial NiO phase, while reduction to Ni prevails at higher temperature.

The "Ni" concentration profile for C-10Ni/$MgAl_2O_4$ (Figure 2C) shows a two-step reduction process in the range 400–800°C, easiest seen as first derivative (Figure S11). 23% of NiO

reduces in the range 400–550°C, followed by 74% in the latter part of TPR, up to a total of 97%. While the first step lies within the temperature window of bare NiO reduction, the second occurs at higher temperature, indicating stronger bound oxygen is removed. The latter provides the interface connection between the NiO particles and the support, i.e. the MSI[31, 36-38]. The first reduction peak then pertains to removal of O with little or no support interaction, e.g. at larger distance from the interface. The residual 3±0.5% unreduced NiO at the end of TPR is due to the last MSI at the interface, maintaining bonds to the support even after prolonged reduction[17, 39-40].

After H_2-TPR, C-10Ni/$MgAl_2O_4$ was cooled down in H_2 for comparison of the reduced and as-prepared state. The EXAFS signature (Figure S12) is adequately described using Ni-Ni (metallic Ni) scattering paths (Table S3). Again, the CN value of 8.2±0.5 is notably lower than the one for bulk FCC Ni, illustrating the beneficial effect of MSI in retaining NP dispersion after treatment at high temperature[41-42]. Ni-O paths from the residual 3% NiO are not resolved in the EXAFS data post H_2-TPR due to their low fraction.

Unlike bare NiO, CO_2 exposure does re-oxidize the $MgAl_2O_4$-supported Ni^0 back to Ni^{2+} (Figure 2D). PCA (Figure S13) and MCR-ALS (Figure 2E-F) quantify this re-oxidation as single-step Ni → NiO within the range 270–600°C (Figure S14, Table S4). The RT EXAFS signature post TPO (Figure S15) further validates the complete re-oxidation of Ni. The observed oxidation degree cannot result from possible impurities present in the used CO_2 bottle (alpha grade, N53), which are too low in quantity, hence the re-oxidation must originate from the admitted CO_2.

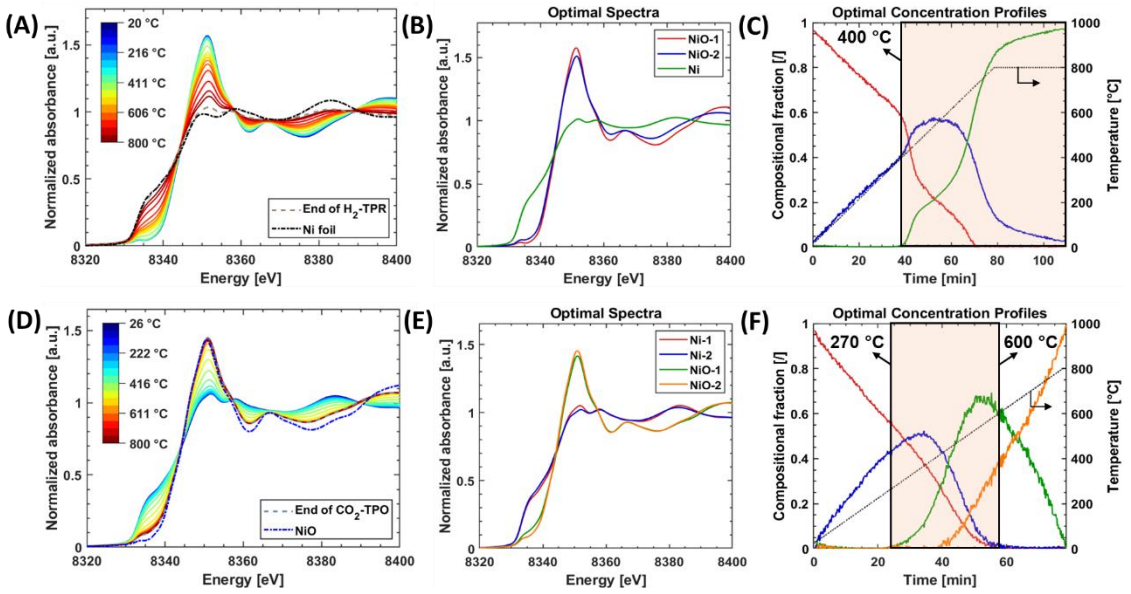

Figure 2. In-situ Ni K-edge QXAS for C-10Ni/$MgAl_2O_4$. (A) XANES during H_2-TPR. (B) MCR-ALS component spectra and (C) concentration profiles, extracted from the QXAS H_2-TPR dataset. (D) XANES during CO_2-TPO of "reduced" C-10Ni/$MgAl_2O_4$. (E) MCR-ALS component spectra and (F) concentration profiles, extracted from the QXAS CO_2-TPO dataset. Light orange: reduction/oxidation windows, vertical black lines: temperature borders.

Based on comparison of the H_2-CO_2 redox behavior, $MgAl_2O_4$-supported NiO differentiates from bare NiO in 2 ways: (1) its reduction temperature lies significantly higher and (2) Ni re-oxidation occurs for C-10Ni/$MgAl_2O_4$, while it does not for unsupported material. The effect of the support was further examined through 'conventional' H_2-TPR and CO_2-TPO in sequence (details in SI).

Benchmark experiments were first conducted for $MgAl_2O_4$, NiO and a mechanical mixture thereof (Figure S16). H_2 consumption by the support is negligible up to 800°C, in accordance with previous reports[38, 43]. The TPR profile of bulk NiO agrees with published work[44], while the one for the NiO-$MgAl_2O_4$ mixture is quasi-identical, except for a small peak at 261°C. The latter is ascribed to H_2 activation, facilitated by the contacting points between the two compounds. No notable re-oxidation by CO_2 was found for bulk NiO –in line with QXAS (Figure 1D)– or for the mechanical mixture of bulk NiO and support. Hence, mere physical

interaction between NiO and $MgAl_2O_4$ does not yield additional redox properties compared to bare NiO.

In H_2-TPR, all as-prepared supported materials exhibit a reduction peak in the range 700–800°C (Figure 3A, Table S5). Based on the XAS analysis for C-10Ni/$MgAl_2O_4$ (Figure S11), this stems from O removal at the interface, where NiO interacts strongly with the support. Another reduction peak around 450-500°C, representing weaker support interaction, dominates for WI-40Ni/$MgAl_2O_4$, while being less intense for WI-20Ni/$MgAl_2O_4$. Since this peak grows with NiO loading and particle size (Table S1), it rather pertains to reduction of the particle itself, with less influence from the support.

Complete re-oxidation by CO_2-TPO occurs for C-10Ni/$MgAl_2O_4$, WI-5Ni/$MgAl_2O_4$ and WI-10Ni/$MgAl_2O_4$, as indicated by the similar H_2 uptake in their 1st and 2nd TPR (Figure 3B). For WI-20Ni/$MgAl_2O_4$ and WI-40Ni/$MgAl_2O_4$, re-oxidation regains only half or less of the as-prepared state and is mostly limited to the stronger bound oxygen at the interface.

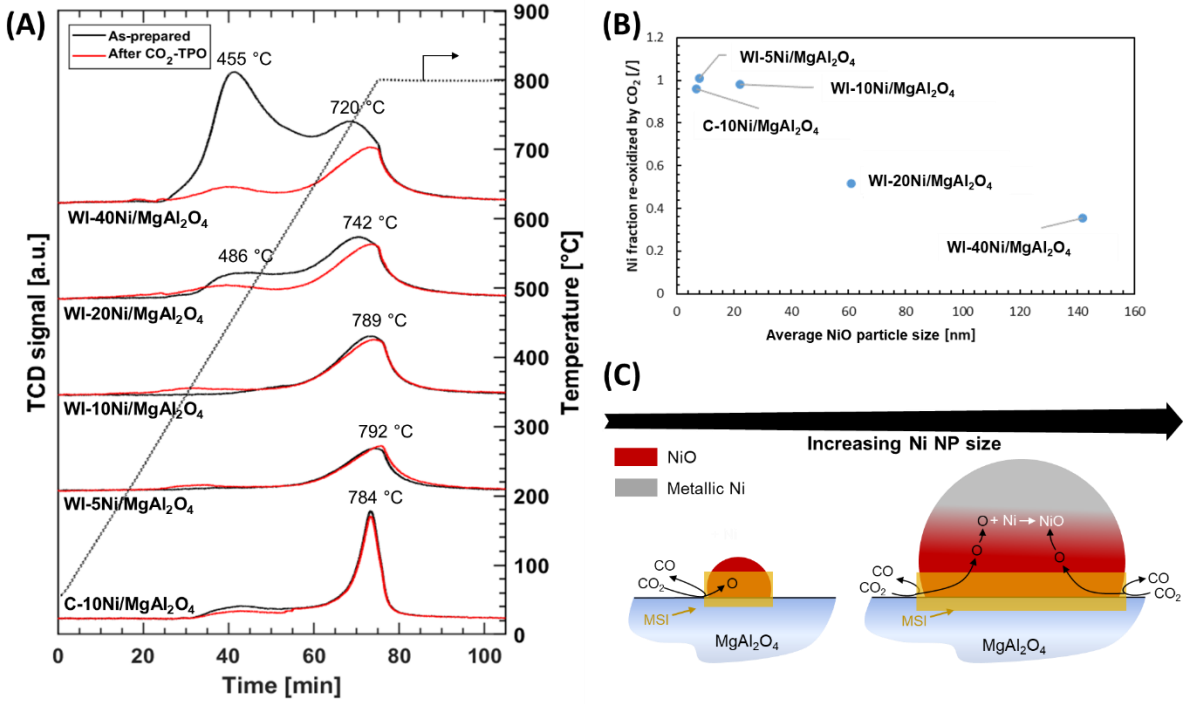

Figure 3. (A) H_2-TPR for $Ni/MgAl_2O_4$ materials recorded "as-prepared" (black) and "after CO_2-TPO" (red). (B) Fraction of Ni re-oxidation after CO_2-TPO as a function of average NiO NP size, determined from TCD H_2-TPR data and TEM. (C) Schematic of $Ni/MgAl_2O_4$ re-oxidation by CO_2.

These observations can be explained by the extent of MSI between Ni and the support. For smaller NPs –$C\text{-}10Ni/MgAl_2O_4$, $WI\text{-}5Ni/MgAl_2O_4$ and $WI\text{-}10Ni/MgAl_2O_4$ (Table S1)– the interface area between Ni and the support is relatively large. The small size of the NiO particles entails that the majority of their oxygen atoms experiences MSI, leading to a dominant high temperature reduction peak. When the NiO particles grow larger, in $WI\text{-}20Ni/MgAl_2O_4$ and $WI\text{-}40Ni/MgAl_2O_4$, more O are located beyond the influence of support interaction, inducing a transition towards a dominant low temperature reduction peak, which reflects less or no MSI.

Ni re-oxidation by CO_2 most easily takes place at sites where MSI exist between Ni and $MgAl_2O_4$. Foppa et al.[45] reported that CO_2 activation on Ni/Al_2O_3 catalysts preferably occurs at the $Ni\text{-}Al_2O_3$ interface. Silaghi and co-workers[46] also denoted the Ni-support interface as the most energetically favorable site for CO_2 activation, resulting in the formation of adsorbed CO

and oxygen species, which react with Ni to form NiO. A similar mechanism is thus proposed for Ni/$MgAl_2O_4$. Although CO_2 can adsorb dissociatively over the entire Ni surface, it will also readily recombine. The Ni-$MgAl_2O_4$ interface however, offers active adsorption sites[46] together with a diffusion channel for O into Ni. Hence, O gets withdrawn from the interface, leading to diffusion-controlled re-oxidation: first locally at and close to the interface, i.e. the highest reduction peak in Figure 3A, next, also further away from the interface, after oxygen diffusion. In case of larger particles, i.e. WI-20Ni/$MgAl_2O_4$ and WI-40Ni/$MgAl_2O_4$, the supply of oxygen from the interface to the rest of the particle is hindered by this diffusion, such that oxidation by the CO_2-derived oxygen species fades out gradually when moving away from the interface (Figure 3C). As MSI-related activation is absent in bulk Ni and the reduced mechanical mixture, re-oxidation by CO_2 is virtually non-existent within the TPO timeframe. In materials with weaker MSI, e.g. WI-10Ni/SiO_2, the interface is less favorable to CO_2 activation, entailing only partial re-oxidation during CO_2-TPO (Figure S17 and Table S5), in strong contrast to the quasi-complete re-oxidation of WI-10Ni/$MgAl_2O_4$.

In summary, a combination of in-situ QXAS, coupled with MCR-ALS, and 'conventional' H_2-TPR and CO_2-TPO experiments shows that bare Ni cannot be oxidized by CO_2, while $MgAl_2O_4$-supported Ni can. The Ni-$MgAl_2O_4$ interface, showing MSI, provides active sites for CO_2 activation and a channel for Ni re-oxidation. This oxidation evolves away from the interface, steered by oxygen diffusion. Within the CO_2-TPO timeframe, complete oxidation only occurs for small supported NPs. This work not only underlines the significance of support effects in Ni-based materials, but also provides a fundamental understanding of the separate effect of CO_2 on Ni/$MgAl_2O_4$, contributing towards the design of more active Ni-based catalysts and more detailed kinetic models for these catalysts.

ASSOCIATED CONTENT

Supporting Information.

The Supporting Information is available free of charge at https://pubs.acs.org. Materials and methods; dynamic light scattering data of Ni colloid; XRD; Electron microscopy results; PCA and MCR-ALS goodness of fit results of QXAS data; EXAFS modelling results and structural parameters of as-prepared, reduced and oxidized states, and MCR-ALS components; H_2-TPR profiles of bulk NiO, $MgAl_2O_4$ and mechanical mixture; quantitative H_2-TPR data for Ni/$MgAl_2O_4$ and WI-10Ni/SiO_2; H_2-TPR profiles of WI-10Ni/SiO_2. (PDF)

AUTHOR INFORMATION

Notes

The authors declare no competing financial interests.

ACKNOWLEDGMENTS

V.D.C. acknowledges a personal grant from the Research Fund of Ghent University (BOF; 01D00719). The research leading to these results has been supported by the project CALIPSOplus under Grant Agreement 730872 from the EU Framework Programme for Research and Innovation HORIZON 2020, in supplying financing of subsistence costs for the synchrotron campaign (SOLEIL, proposal 20200555). The authors acknowledge the assistance from the ROCK staff for a smooth beamtime. This work was supported by a public grant overseen by the French National Research Agency (ANR) as part of the "Investissements d'Avenir" program (reference: ANR-10-EQPX-45).

REFERENCES

1. Usman, M.; Wan Daud, W. M. A.; Abbas, H. F. Dry reforming of methane: Influence of process parameters—A review. *Renew. Sustain. Energy Rev.* **2015,** *45*, 710-744.
2. Aramouni, N. A. K.; Touma, J. G.; Tarboush, B. A.; Zeaiter, J.; Ahmad, M. N. Catalyst design for dry reforming of methane: Analysis review. *Renew. Sustain. Energy Rev.* **2018,** *82*, 2570-2585.
3. Pakhare, D.; Spivey, J. A review of dry (CO_2) reforming of methane over noble metal catalysts. *Chem. Soc. Rev.* **2014,** *43*, 7813-7837.
4. Yang, H.; Zhang, C.; Gao, P.; Wang, H.; Li, X.; Zhong, L.; Wei, W.; Sun, Y. A review of the catalytic hydrogenation of carbon dioxide into value-added hydrocarbons. *Catal. Sci. Technol.* **2017**, *7*, 4580-4598.
5. Saeidi, S.; Amin, N. A. S.; Rahimpour, M. R. Hydrogenation of CO_2 to value-added products—A review and potential future developments. *J. CO_2 Util.* **2014,** *5*, 66-81.
6. Wang, W.; Wang, S.; Ma, X.; Gong, J. Recent advances in catalytic hydrogenation of carbon dioxide. *Chem. Soc. Rev.* **2011,** *40*, 3703-3727.
7. Abdullah, B.; Abd Ghani, N. A.; Vo, D.-V. N. Recent advances in dry reforming of methane over Ni-based catalysts. *J. Clean. Prod.* **2017,** *162*, 170-185.
8. Seo, H. O. Recent Scientific Progress on Developing Supported Ni Catalysts for Dry (CO_2) Reforming of Methane. *Catalysts* **2018,** *8*, 110.
9. Le, T. A.; Kim, M. S.; Lee, S. H.; Kim, T. W.; Park, E. D. CO and CO_2 methanation over supported Ni catalysts. *Catal. Today* **2017,** *293-294*, 89-96.
10. Alrafei, B.; Polaert, I.; Ledoux, A.; Azzolina-Jury, F. Remarkably stable and efficient Ni and Ni-Co catalysts for CO_2 methanation. *Catal. Today* **2020,** *346*, 23-33.
11. Ye, R.-P.; Li, Q.; Gong, W.; Wang, T.; Razink, J. J.; Lin, L.; Qin, Y.-Y.; Zhou, Z.; Adidharma, H.; Tang, J.; Russell, A. G.; Fan, M.; Yao, Y.-G. High-performance of nanostructured Ni/CeO_2 catalyst on CO_2 methanation. *Appl. Catal. B: Environ.* **2020,** *268*, 118474.
12. Mutz, B.; Belimov, M.; Wang, W.; Sprenger, P.; Serrer, M.-A.; Wang, D.; Pfeifer, P.; Kleist, W.; Grunwaldt, J.-D. Potential of an Alumina-Supported Ni_3Fe Catalyst in the Methanation of CO_2: Impact of Alloy Formation on Activity and Stability. *ACS Catal.* **2017,** *7*, 6802-6814.
13. Theofanidis, S. A.; Galvita, V. V.; Poelman, H.; Marin, G. B. Enhanced Carbon-Resistant Dry Reforming Fe-Ni Catalyst: Role of Fe. *ACS Catal.* **2015,** *5*, 3028-3039.
14. Vesselli, E.; Rizzi, M.; De Rogatis, L.; Ding, X.; Baraldi, A.; Comelli, G.; Savio, L.; Vattuone, L.; Rocca, M.; Fornasiero, P.; Baldereschi, A.; Peressi, M. Hydrogen-Assisted Transformation of CO_2 on Nickel: The Role of Formate and Carbon Monoxide. *J. Phys. Chem. Lett.* **2010,** *1*, 402-406.
15. Wang, H.; Lu, J. A Review on Particle Size Effect in Metal-Catalyzed Heterogeneous Reactions. *Chin. J. Chem .* **2020,** *38*, 1422-1444.
16. Pan, C.-J.; Tsai, M.-C.; Su, W.-N.; Rick, J.; Akalework, N. G.; Agegnehu, A. K.; Cheng, S.-Y.; Hwang, B.-J. Tuning/exploiting Strong Metal-Support Interaction (SMSI) in Heterogeneous Catalysis. *J. Taiwan Inst. Chem. Eng.* **2017,** *74*, 154-186.
17. Divins, N. J.; Angurell, I.; Escudero, C.; Pérez-Dieste, V.; Llorca, J. Influence of the support on surface rearrangements of bimetallic nanoparticles in real catalysts. *Science* **2014,** *346*, 620.
18. Ahmadi, M.; Mistry, H.; Roldan Cuenya, B. Tailoring the Catalytic Properties of Metal Nanoparticles via Support Interactions. *J. Phys. Chem. Lett.* **2016,** *7*, 3519-3533.
19. Song, T.; Dong, J.; Li, R.; Xu, X.; Hiroaki, M.; Yang, B.; Zhang, R.; Bai, Y.; Xin, H.; Lin, L.; Mu, R.; Fu, Q.; Bao, X. Oxidative Strong Metal–Support Interactions between Metals and Inert Boron Nitride. *J. Phys. Chem. Lett.* **2021,** *12*, 4187-4194.
20. Kesavan, J. K.; Luisetto, I.; Tuti, S.; Meneghini, C.; Iucci, G.; Battocchio, C.; Mobilio, S.; Casciardi, S.; Sisto, R. Nickel supported on YSZ: The effect of Ni particle size on the catalytic activity for CO_2 methanation. *J. CO_2 Util.* **2018,** *23*, 200-211.
21. Wierzbicki, D.; Baran, R.; Dębek, R.; Motak, M.; Gálvez, M. E.; Grzybek, T.; Da Costa, P.; Glatzel, P. Examination of the influence of La promotion on Ni state in hydrotalcite-derived catalysts

under CO_2 methanation reaction conditions: Operando X-ray absorption and emission spectroscopy investigation. *Appl. Catal. B: Environ.* **2018,** *232*, 409-419.
22. Lee, Y. H.; Ahn, J. Y.; Nguyen, D. D.; Chang, S. W.; Kim, S. S.; Lee, S. M. Role of oxide support in Ni based catalysts for CO_2 methanation. *RSC Adv.* **2021,** *11*, 17648-17657.
23. Sheng, Z.; Kameshima, S.; Yao, S.; Nozaki, T. Oxidation behavior of Ni/Al_2O_3 catalyst in nonthermal plasma-enabled catalysis. *J. Phys. D: Appl. Phys.* **2018,** *51*, 445205.
24. Mutz, B.; Gänzler, A. M.; Nachtegaal, M.; Müller, O.; Frahm, R.; Kleist, W.; Grunwaldt, J.-D. Surface Oxidation of Supported Ni Particles and Its Impact on the Catalytic Performance during Dynamically Operated Methanation of CO_2. *Catalysts* **2017,** *7*, 279.
25. Chen, W.; Zhao, G.; Xue, Q.; Chen, L.; Lu, Y. High carbon-resistance $Ni/CeAlO_3$-Al_2O_3 catalyst for CH_4/CO_2 reforming. *Appl. Catal. B: Environ.* **2013,** *136-137*, 260-268.
26. Yuan, K.; Zhong, J.-Q.; Zhou, X.; Xu, L.; Bergman, S. L.; Wu, K.; Xu, G. Q.; Bernasek, S. L.; Li, H. X.; Chen, W. Dynamic Oxygen on Surface: Catalytic Intermediate and Coking Barrier in the Modeled CO_2 Reforming of CH_4 on Ni (111). *ACS Catal.* **2016,** *6*, 4330-4339.
27. Sehested, J. Four challenges for nickel steam-reforming catalysts. *Catal. Today* **2006,** *111*, 103-110.
28. Koo, K. Y.; Roh, H.-S.; Seo, Y. T.; Seo, D. J.; Yoon, W. L.; Bin Park, S. A highly effective and stable nano-sized $Ni/MgO–Al_2O_3$ catalyst for gas to liquids (GTL) process. *Int. J. Hydrogen Energy* **2008,** *33*, 2036-2043.
29. Guo, J.; Lou, H.; Zhao, H.; Wang, X.; Zheng, X. Novel synthesis of high surface area $MgAl_2O_4$ spinel as catalyst support. *Mater. Lett.* **2004,** *58*, 1920-1923.
30. Guo, J.; Lou, H.; Zhao, H.; Chai, D.; Zheng, X. Dry reforming of methane over nickel catalysts supported on magnesium aluminate spinels. *Appl. Catal. A: Gen.* **2004,** *273*, 75-82.
31. Hadian, N.; Rezaei, M.; Mosayebi, Z.; Meshkani, F. CO_2 reforming of methane over nickel catalysts supported on nanocrystalline $MgAl_2O_4$ with high surface area. *J. Nat. Gas Chem.* **2012,** *21*, 200-206.
32. Alvar, E. N.; Rezaei, M. Mesoporous nanocrystalline $MgAl_2O_4$ spinel and its applications as support for Ni catalyst in dry reforming. *Scripta Mater.* **2009,** *61*, 212-215.
33. Fan, Z.; Sun, K.; Rui, N.; Zhao, B.; Liu, C.-j. Improved activity of $Ni/MgAl_2O_4$ for CO_2 methanation by the plasma decomposition. *J. Energy Chem.* **2015,** *24*, 655-659.
34. Vrijburg, W. L.; van Helden, J. W. A.; van Hoof, A. J. F.; Friedrich, H.; Groeneveld, E.; Pidko, E. A.; Hensen, E. J. M. Tunable colloidal Ni nanoparticles confined and redistributed in mesoporous silica for CO_2 methanation. *Catal. Sci. Technol.* **2019,** *9*, 2578-2591.
35. De Coster, V.; Poelman, H.; Dendooven, J.; Detavernier, C.; Galvita, V. V. Designing Nanoparticles and Nanoalloys for Gas-Phase Catalysis with Controlled Surface Reactivity Using Colloidal Synthesis and Atomic Layer Deposition. *Molecules* **2020,** *25*, 3735.
36. Hadian, N.; Rezaei, M. Combination of dry reforming and partial oxidation of methane over Ni catalysts supported on nanocrystalline $MgAl_2O_4$. *Fuel* **2013,** *113*, 571-579.
37. Mosayebi, Z.; Rezaei, M.; Ravandi, A. B.; Hadian, N. Autothermal reforming of methane over nickel catalysts supported on nanocrystalline $MgAl_2O_4$ with high surface area. *Int. J. Hydrogen Energy* **2012,** *37*, 1236-1242.
38. Shen, J.; Reule, A. A. C.; Semagina, N. $Ni/MgAl_2O_4$ catalyst for low-temperature oxidative dry methane reforming with CO_2. *Int. J. Hydrogen Energy* **2019,** *44*, 4616-4629.
39. Shi, X. Y.; Zhang, W.; Zhang, C.; Zheng, W. T.; Chen, H.; Qi, J. G. Real-space observation of strong metal-support interaction: state-of-the-art and what's the next. *J. Microsc.* **2016,** *262*, 203-215.
40. Theofanidis, S. A.; Galvita, V. V.; Poelman, H.; Dharanipragada, N. V. R. A.; Longo, A.; Meledina, M.; Van Tendeloo, G.; Detavernier, C.; Marin, G. B. Fe-Containing Magnesium Aluminate Support for Stability and Carbon Control during Methane Reforming. *ACS Catal.* **2018,** *8*, 5983-5995.
41. Haddad, G. J.; Chen, B.; Goodwin, J. J. G. Characterization of La^{3+}-Promoted Co/SiO_2 Catalysts. *J. Catal.* **1996,** *160*, 43-51.

42. Li, X.; Zhang, Y.; Smith, K. J. Metal–support interaction effects on the growth of filamentous carbon over Co/SiO_2 catalysts. *Appl. Catal. A: Gen.* **2004,** *26*4, 81-91.
43. Jeong, J. H.; Lee, J. W.; Seo, D. J.; Seo, Y.; Yoon, W. L.; Lee, D. K.; Kim, D. H. Ru-doped Ni catalysts effective for the steam reforming of methane without the pre-reduction treatment with H_2. *Appl. Catal. A: Gen.* **2006,** *302*, 151-156.
44. Mette, K.; Kühl, S.; Tarasov, A.; Düdder, H.; Kähler, K.; Muhler, M.; Schlögl, R.; Behrens, M. Redox dynamics of Ni catalysts in CO_2 reforming of methane. *Catal. Today* **2015,** *242*, 101-110.
45. Foppa, L.; Margossian, T.; Kim, S. M.; Müller, C.; Copéret, C.; Larmier, K.; Comas-Vives, A. Contrasting the Role of Ni/Al_2O_3 Interfaces in Water–Gas Shift and Dry Reforming of Methane. *J. Am. Chem. Soc.* **2017,** *139*, 17128-17139.
46. Silaghi, M.-C.; Comas-Vives, A.; Copéret, C. CO_2 Activation on Ni/γ–Al_2O_3 Catalysts by First-Principles Calculations: From Ideal Surfaces to Supported Nanoparticles. *ACS Catal.* **2016,** *6*, 4501-4505.